

Article

Experimental Investigation on Failure Mechanisms of HDPE Welded Geocell Junctions under Different Clamping Distances

Guangqing Yang^{1,2}, Penghui Su^{1,3,*}, Peng Xu^{1,2}, Zhijie Wang^{1,2}, He Wang^{1,2} and Zheng Zuo^{1,3} 

- ¹ State Key Laboratory of Mechanical Behavior and System Safety of Traffic Engineering Structures, Shijiazhuang Tiedao University, Shijiazhuang 050043, China; yanggq@stdu.edu.cn (G.Y.); sdxplt@163.com (P.X.); zwang@stdu.edu.cn (Z.W.); wanghe@stdu.edu.cn (H.W.); geozz@stdu.edu.cn (Z.Z.)
- ² School of Civil Engineering, Shijiazhuang Tiedao University, Shijiazhuang 050043, China
- ³ School of Traffic and Transportation, Shijiazhuang Tiedao University, Shijiazhuang 050043, China
- * Correspondence: 2202106004@student.stdu.edu.cn

Abstract: Geocells are three-dimensional honeycomb-reinforced geotechnical materials composed of strips and junctions. Its junctions can support and transmit forces in several directions. The performance of geocells has a considerable impact on engineering applications. However, the testing program of geocell junctions still lacks standardization, and limited research has been undertaken regarding the failure mechanisms of junctions when subjected to various stress types. In this paper, four test procedures for HDPE welded geocell junctions were performed, including weld tensile, shear, peeling, and splitting strength tests. The influence of tests under different clamping distances (10.5 mm, 25 mm, 50 mm, and 100 mm) was analyzed, and the stress–strain behavior, peak elongation, and peak and residual strength of junctions under various force states were analyzed in detail. Finally, considering the strength and deformation, the slope laying method of geocells was proposed. The results show that the tensile strength and shear strength decrease with the clamping distance, whereas the peeling strength and splitting strength remain essentially unchanged. Under a 100 mm clamping distance, the tensile strength and shear strength are decreased by 4.51% and 14.08%. Geocells spreading vertically along the surface on a subgrade slope are thought to be more reliable, improving the geocell’s service life in slope protection. The test results can be used to improve a standardized geocell junction testing procedure as well as to guide, evaluate, and enhance the quality and application dependability of geocells.

Keywords: HDPE welded geocell; junction; tensile test; clamping distance; failure mechanism



Citation: Yang, G.; Su, P.; Xu, P.; Wang, Z.; Wang, H.; Zuo, Z. Experimental Investigation on Failure Mechanisms of HDPE Welded Geocell Junctions under Different Clamping Distances. *Appl. Sci.* **2022**, *12*, 5343. <https://doi.org/10.3390/app12115343>

Academic Editor: José A.F.O. Correia

Received: 12 May 2022

Accepted: 23 May 2022

Published: 25 May 2022

Publisher’s Note: MDPI stays neutral with regard to jurisdictional claims in published maps and institutional affiliations.



Copyright: © 2022 by the authors. Licensee MDPI, Basel, Switzerland. This article is an open access article distributed under the terms and conditions of the Creative Commons Attribution (CC BY) license (<https://creativecommons.org/licenses/by/4.0/>).

1. Introduction

Geocells have been widely utilized in geotechnical engineering for a long time due to their effective reinforcement performance and obvious economic benefits, such as pavement [1–3], embankment [4], foundation [5,6], and slope protection [7,8]. The geocell’s three-dimensional honeycomb structure provides more lateral constraints than other planar reinforcement materials, which, when combined with the filling material, shapes a composite reinforcement with high strength and stability, further improving the structure’s overall reliability and service life [9].

Hegde [10] found, by means of a compression test, that the junction was the key factor in the geocell’s “ferrule effect”. Isik and Gurbuz [11] conducted indoor pull-out experiments for geocells and indicated that the pull-out resistance of geocells was limited by the seam peel strength of the geocell junctions. Using the limit equilibrium method (LEM), Khorsandiardebili and Ghazavi [12] provided an analytical approach to investigate the stability of geocell-reinforced slopes. Inti [13] proposed vulnerability modeling to design small volume roads by considering the modulus of the geocell-reinforced layer and showed that geocell reinforcement reduced the stress of the cushion beneath the pavement. Zhao [14] developed the polymer-blend geocell (PBG) and investigated the tensile properties of

blends of various formulations in terms of yield strength, tensile strength, and elongation at break. The above studies focused on the material properties, engineering application, and reinforcement mechanism of geocells, evaluated the performance of geocells extensively, and emphasized the importance of geocell junctions. Therefore, a detailed study of geocell junctions is required to assure the safety and stability of reinforced structures.

Song [15] conducted centrifugal model experiments to investigate the failure mode of the geocell-reinforced soil retaining wall, discovering that the geocell strips were stretched and ruptured and that the connections at the junctions collapsed. Based on laboratory tests and a numerical simulation, Leshchinsky and Ling [16] demonstrated that the junctions played a crucial role under cyclic loads or multiple loads; no tearing or rupture was found on the cell-wall or at the junction. Yang [17] observed the failure of the junction by placing the NPA geocell in the sand base of the unpaved road. By loading unconstrained geocell elements, Pokharel [18] observed similar failure scenarios. Both geocell junctions and strips are subjected to soil action from all directions [19]. Geocells need to withstand high tearing, tensile, and shear stresses in both the strips and the welded junctions to prevent the strips' rupture and separation of the junctions. Some studies have found the failure phenomenon of the geocell junction [15,17,18], but these research results cannot fully explain and evaluate the failure mode and the performance of junctions, hindering the application and promotion of geocells in the engineering field.

In addition, to simulate the different force states of junctions, Zuo [20] compared and analyzed the failure mechanisms of the junctions of welding, bolt, and plug connections under various stress states. The tensile shear, peeling, and splitting tests were conducted with a clamping distance of 100 mm. Liu [21] also studied the response of HDPE welded geocell junctions under different load conditions. The weld tensile strength and tensile shear tests were conducted with a clamping distance of 10.5 mm, and a clamping distance of 30 mm was used for the peeling and splitting tests. However, there is a lack of standardization in the geocell tensile test method, and scholars' test processes differ in terms of the distance of clamps, which could lead to variances in the research on specimen test failure mechanisms and the evaluation of geocell product performance. The design uncertainties and unforeseen failure patterns of junctions have impeded the application of geocells in some engineering fields, such as highway and railway engineering.

Based on the above analysis, considering that the testing program of geocell junctions still lacks uniformity (as there are differences in terms of clamping distance) and that limited research has been undertaken regarding the failure mechanisms of junctions when subjected to various stress modes, a series of tensile tests was carried out for the junctions of HDPE welded geocells commonly used in engineering, including weld tensile, shear, peeling, and splitting strength tests. To study the response of each type of test under different clamping distances, the stress–strain behaviors were measured and recorded along with the peak elongation and peak and residual strength. Different failure characteristics were observed, and the impacts of different clamping distances on each type of test were analyzed. Finally, various types of testing were compared, the correspondences of geocell junctions under different force states were described, the factors affecting the performance of geocell junctions were obtained, and suggestions were provided for the laying mode of geocells on slopes. The test results can provide a reference for establishing the standardized test method of geocell junctions as well as guide, evaluate, and improve the quality and application dependability of geocells. This study is useful in providing test techniques and data support when the real specification of a geocell cannot be tested according to existing standards and the clamping distance needs to be extended or reduced.

2. Materials and Methods

This section summarizes the tests involved in the program. Detailed specimen dimensions, testing schemes, and laboratory procedures are discussed. It should be noted that all sample tests were conducted in accordance with “Geotextiles and geotextile-related products—Strength of internal structural junctions—Part 1: Geocells” (ISO 13426-1-2019)

and “Geosynthetics in railway engineering—Part 1: Geocell” (Q/CR 549.1-2016). The samples were tested by the geosynthetics electronic strength tester (Figure 1) in an environment with a temperature of $(23 \pm 2) ^\circ\text{C}$ and a relative humidity of $(50 \pm 5) \%$ to avoid the influence of environmental factors. During the test, the number of samples prepared for each test scheme was at least 5, and the tensile rate was $50 \text{ mm}\cdot\text{min}^{-1}$.



Figure 1. The geosynthetics electronic strength tester.

2.1. Material

The test samples were commercial geocell products used in subgrade slope protection, as shown in Figure 2. The geocell is made of high-density polyethylene (HDPE), with full-depth and ultrasonic spot-welds used to connect the junctions and aligned perpendicular to the longitudinal axis of the strip. The strip surface has rhomboidal indentations to promote friction with the filling material interface, regular perforation drainage to improve the slope’s drainage capacity, and interlocking with the filling material. Table 1 shows the specifications of the geocell, and Figure 3 presents the details of the geocell junction.

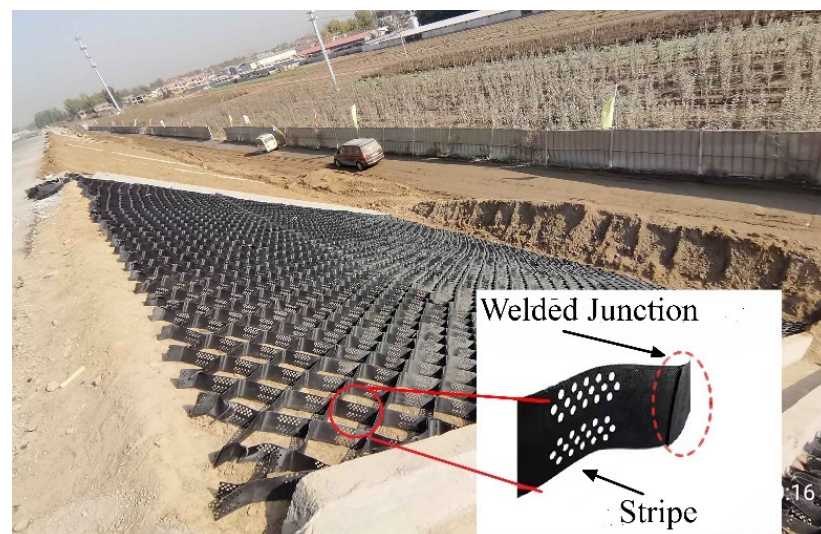
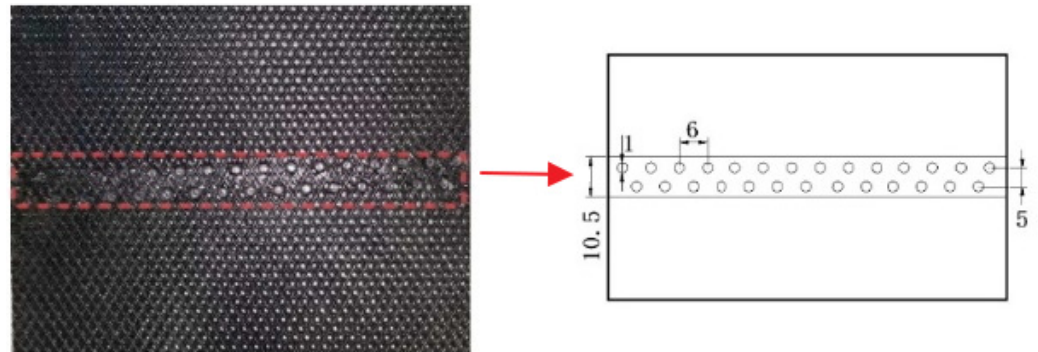


Figure 2. Geocell products for testing.

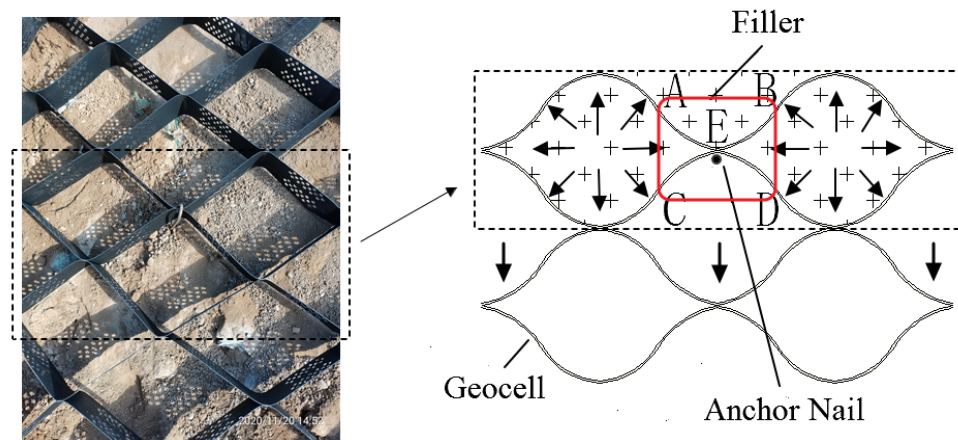
Table 1. Specifications of the geocell.

Connection Mode of the Junctions	Strip Material	Height of the Geocell (mm)	Distance of the Junction (mm)
Ultrasonic welding	HDPE	100	280

**Figure 3.** Details of the geocell junction. (unit: mm).

2.2. Testing Procedures

Geocells are typically subjected to gravity loads from the infill materials on steep slopes [22]. The force diagram of the geocell on the slope is shown in Figure 4. The geocell junctions have the critical features that support and transfer the load. The geocells are affected by the filling materials in all directions, resulting in four forms of failure at the junctions:

**Figure 4.** Schematic diagram of local stress.

1. By local overstressing, the fixation element locally overstresses the junction (in the same way as a tensile test on a welded junction);
2. By shear, a force parallel to the junction itself causes failure;
3. By peeling, a force normal to the junction separates the strips from each other at one edge of the junction, causing failure;
4. By splitting, two strips adjacent to the junction are pulled apart by a force normal to the junction.

Four types of tensile tests were carried out on the geocell junctions. According to “Geosynthetics in railway engineering—Part 1: Geocell” (Q/CR 549.1-2016), the overall length of the sample was 220 mm, the width of the sample was the strip width of the geocell (the height of the geocell), and the clamping distance was 100 mm when the sample was tensioned after the preload was applied. The schematic drawings in Figures 5–8 show the detailed configuration and loading scenario. Combined with the standards and relevant

scholars' research, the distances between clamps of 10.5 mm, 25 mm, 50 mm, and 100 mm were utilized in the experiments to explore the effect of clamping distance on different types of junction tensile testing. These distances ensure that no pre-load is applied to the specimen before the actual test begins. The specimens used in all the tests were initially cut to the correct size for the tensile test. It should be mentioned that stretching with a clamping distance of 10.5 mm was difficult due to the method of the splitting and peeling strength tests, as well as material considerations. Additional samples were tested as necessary to facilitate a high level of consistency. The detailed specimen sizes for the junction test are summarized in Table 2. The types of geocell junction tests include the weld tensile strength, tensile shear, peeling, and splitting tests. This study is intended to supplement and unify test standards as well as to provide a test scheme and data support. There can be a test basis when the geocell specification cannot be tested according to existing standards and the clamping distance needs to be increased or reduced.

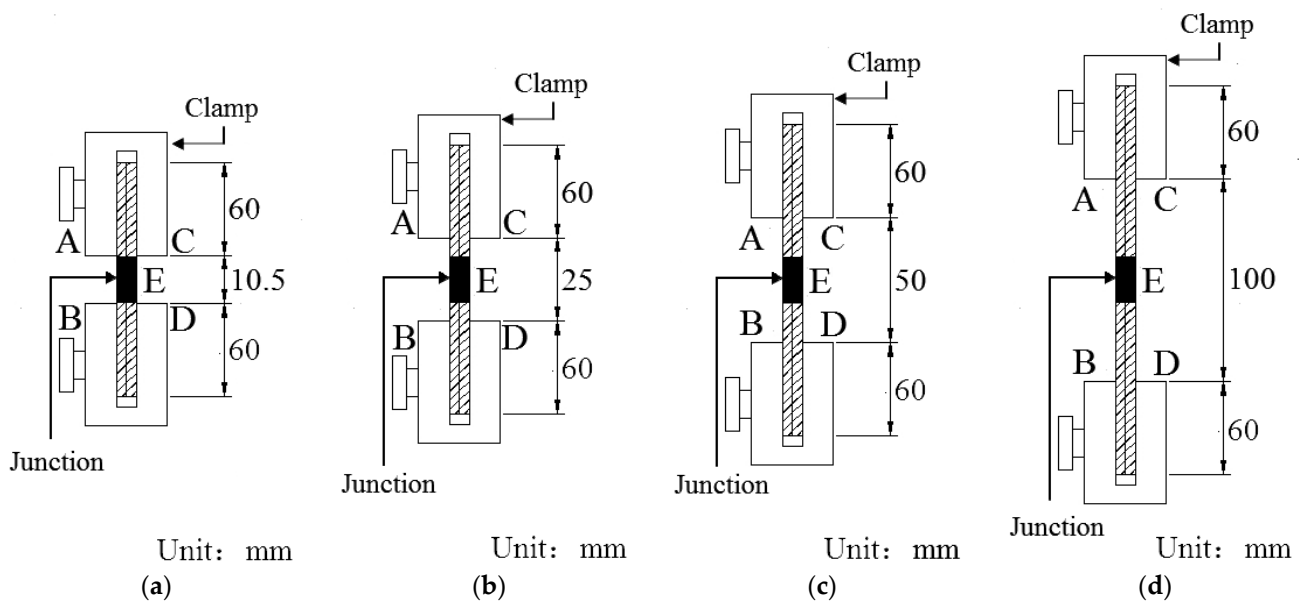


Figure 5. Weld tensile strength tests under different clamping distances: (a) 10.5 mm, (b) 25 mm, (c) 50 mm, (d) 100 mm.

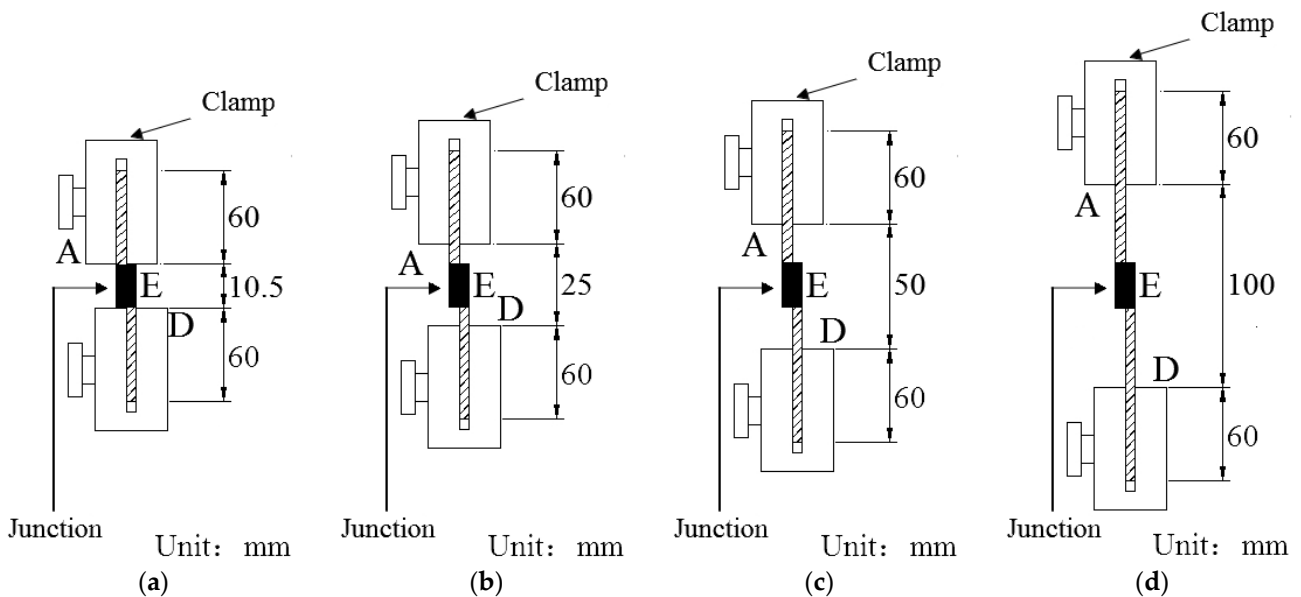


Figure 6. Tensile shear tests under different clamping distances: (a) 10.5 mm, (b) 25 mm, (c) 50 mm, (d) 100 mm.

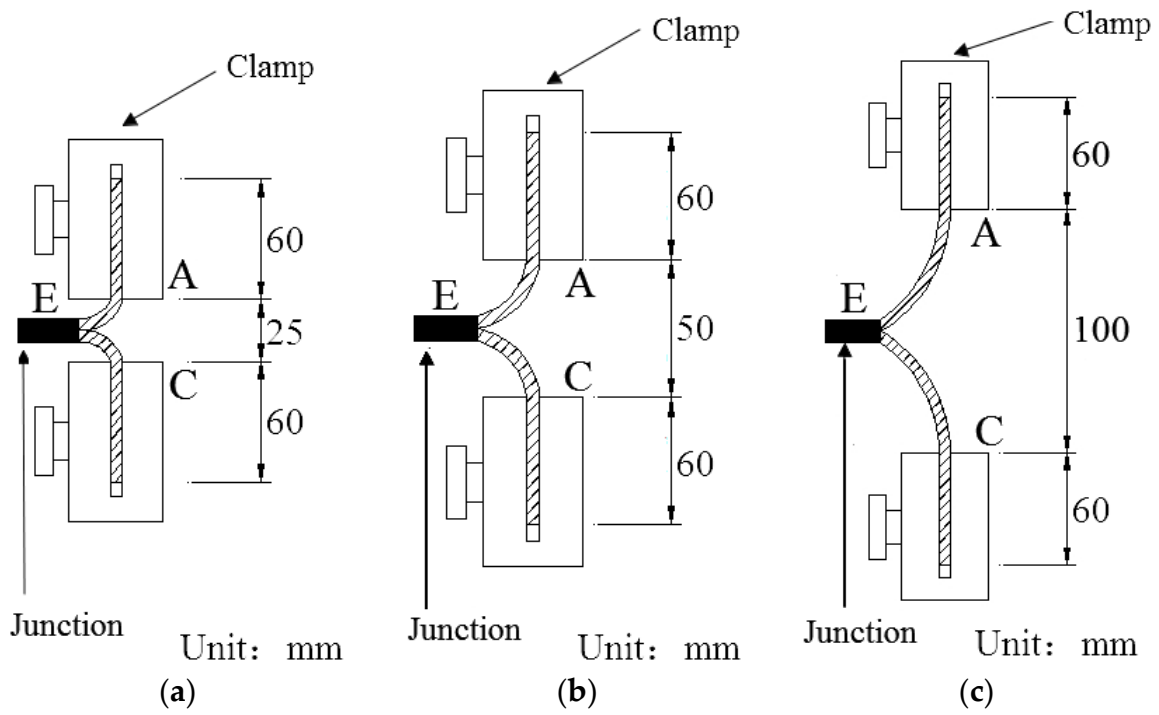


Figure 7. Peeling tests under different clamping distances: (a) 25 mm, (b) 50 mm, (c) 100 mm.

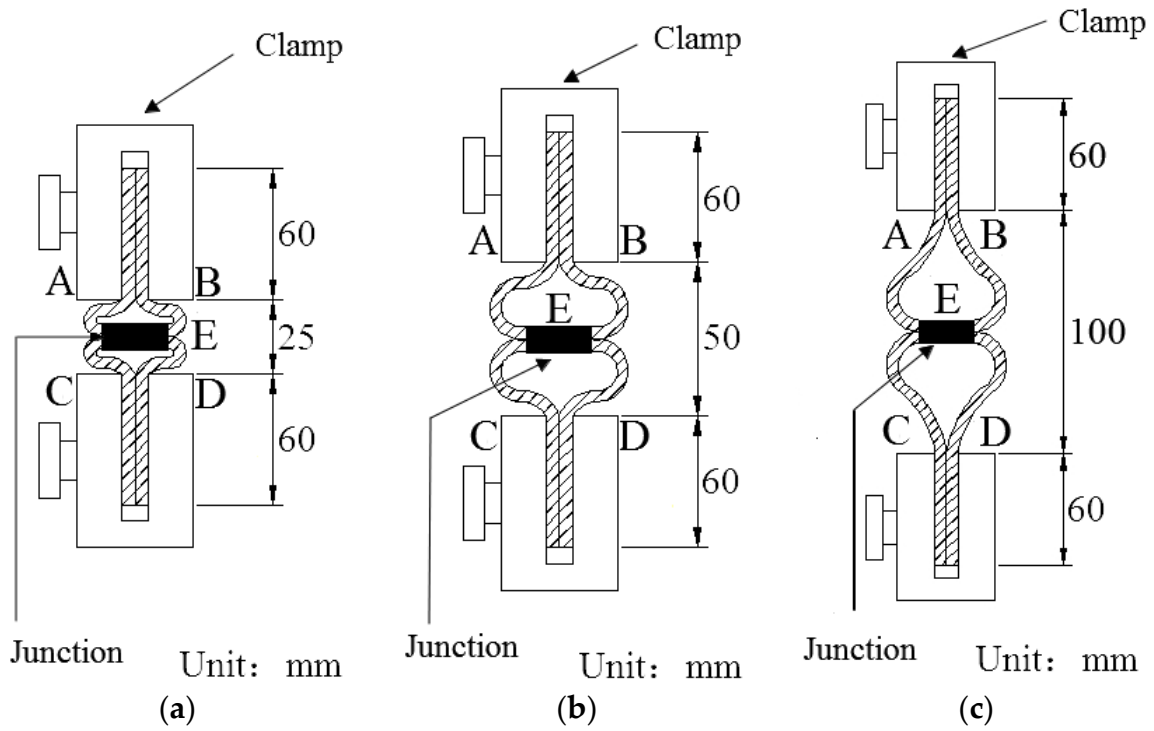


Figure 8. Splitting tests under different clamping distances: (a) 25 mm, (b) 50 mm, (c) 100 mm.

Table 2. Specimen dimensions.

Test	Junction Width (mm)	Clamping Distance (mm)	Gripping Distance (mm)	Overall Length (mm)
Weld tensile strength test		10.5		130.5
		25		145
		50		170
		100		220
Tensile shear test	100	10.5		130.5
		25		145
		50		170
		100	60	220
Peeling test		25		145
		50		170
		100		220
Splitting test		25		145
		50		170
		100		220

All the test methods were designed in reference to “Geotextiles and geotextile-related products—Strength of internal structural junctions—Part 1: Geocells” (ISO 13426-1-2019), and all the tests were performed on an X-shaped sample cut from the geocell panel (Figure 4; red surrounding area).

1. Method A—Weld tensile strength test (Figure 5d)

The legs A and C of the “X” are fixed in the in the upper clamp, and the legs B and D are similarly fixed in the bottom clamp. The sample is tested at a constant tensile rate by adjusting the clamping distance until the junction is plasticized and damaged.

2. Method B—Tensile shear test (Figure 6d)

The right upper leg B and the left lower leg C of “X” are trimmed close to the junction, and the remaining legs A and D are fixed in the upper and lower clamps. The sample is tested at a constant tensile shear rate by adjusting the clamping distance until a shear failure of the junction occurs.

3. Method C—Peeling test (Figure 7c)

The lower legs B and D of “X” are trimmed close to the junction, and the remaining legs A and C are fixed in the upper and lower clamps. The sample is tested at a constant peel rate by adjusting the clamping distance until a peel failure of the junction occurs.

4. Method D—Splitting test (Figure 8c)

The legs A and B of the “X” are fixed in the upper clamp, and the legs C and D are similarly fixed in the bottom clamp. The sample is tested at a constant splitting rate by adjusting the clamping distance until a tensile split failure of the junction occurs.

3. Result and Discussion

This section summarizes the results of the various test processes on the geocell junctions. Due to the complexity of the tensile pattern, the results are presented in the form of engineering stress–elongation, and the test strengths are expressed in N/cm. The significance of the discussion outcomes is linked to the geocell’s practical applicability.

3.1. Weld Tensile Strength Test

Table 3 shows the test results for the weld tensile strength of junctions at different clamping distances. The results indicate that the tensile strengths of the 25 mm, 50 mm, and 100 mm clamping distances are lowered by 0.23%, 2.84%, and 4.51% when compared to the test with the 10.5 mm clamping distance. Compared with the 10.5 mm clamping distance, the peak and overall elongation of the 25 mm clamping distance increased by

30.68% and 13.91%. The peak and overall elongation of the 50 mm clamping distance increased by 50.23% and 18.69% compared with the 25 mm clamping distance. Compared to the 50 mm clamping distance, the peak and overall elongation of the 100 mm clamping distance increased by 105.00% and 31.14%. On the whole, the weld tensile strength of the junction decreases, and the peak and overall elongation increase with the distance between clamps. The change in peak elongation becomes more apparent.

Table 3. Weld tensile test results of the junctions.

Clamping Distance (mm)	Tensile Strength ($\text{N}\cdot\text{cm}^{-1}$)	Peak Elongation (mm)	Overall Elongation (mm)
10.5	350.794	3.592	14.366
25	349.98	4.694	16.364
50	340.82	7.052	19.422
100	334.97	14.456	25.47

The tensile stress–elongation relationship curves of the junctions under different clamping distances are shown in Figure 9. When the strip appears and lengthens, the curve of the elastic area pre-peak slows down, requiring more elongation to attain peak strength, and the strength diminishes faster when broken post-peak. This can be attributed to the fact that the junction and strip are under common stress during the tensile process, and their mechanical behavior is considerably different. The deformation of the junctions is greatly different from that of the strips, and the tensile forces that the junctions and strips can withstand are different. As a whole, they must work together to coordinate their differences, resulting in reduced tensile strength and increased elongation. The increase in overall elongation was due to an increase in the elongation of the pre-peak elastic area.

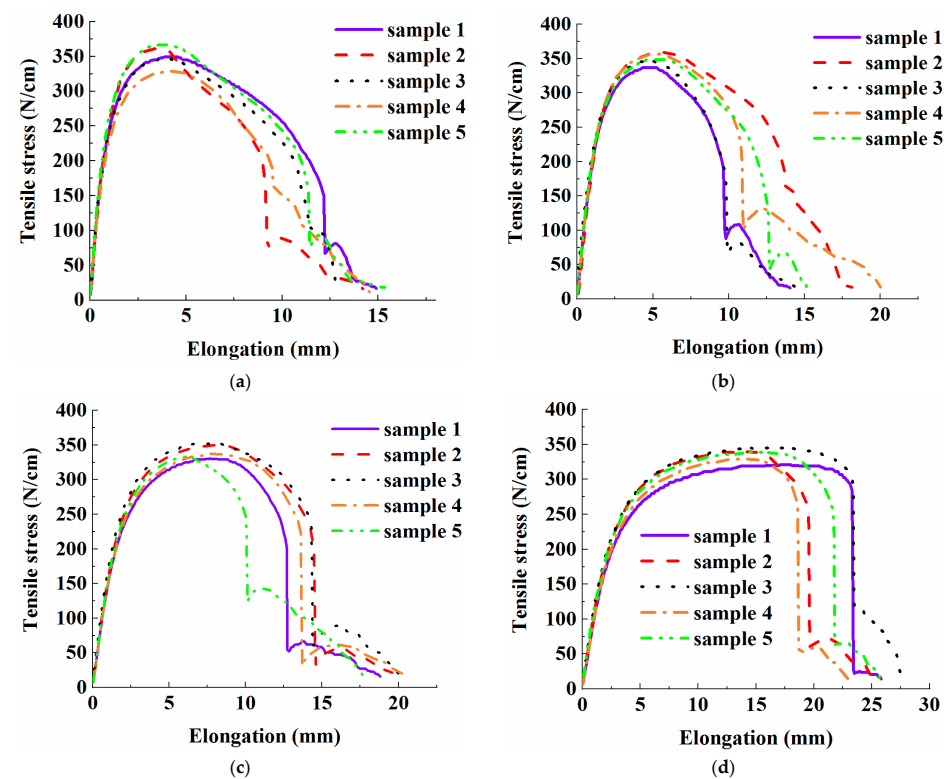


Figure 9. Tensile stress–elongation relationship of the junction subjected to uniaxial tension under various clamping distances: (a) 10.5 mm, (b) 25 mm, (c) 50 mm, (d) 100 mm.

The failure modes of the junctions under tensile loading at different clamping distances can be observed in Figure 10. The failure modes of all the samples are similar. The fractures

occurred at the spot-welding junction, and the strips had no visible change. This indicates that, during the tensile test, when the geocell strip has not begun to deform significantly, the junction is damaged first, and the strip's stress has not reached its yield strength, which is consistent with the results reported by Tarip [23], where they found that the welded junction has a lower tensile strength than the high-density polyethylene (HDPE) material itself.

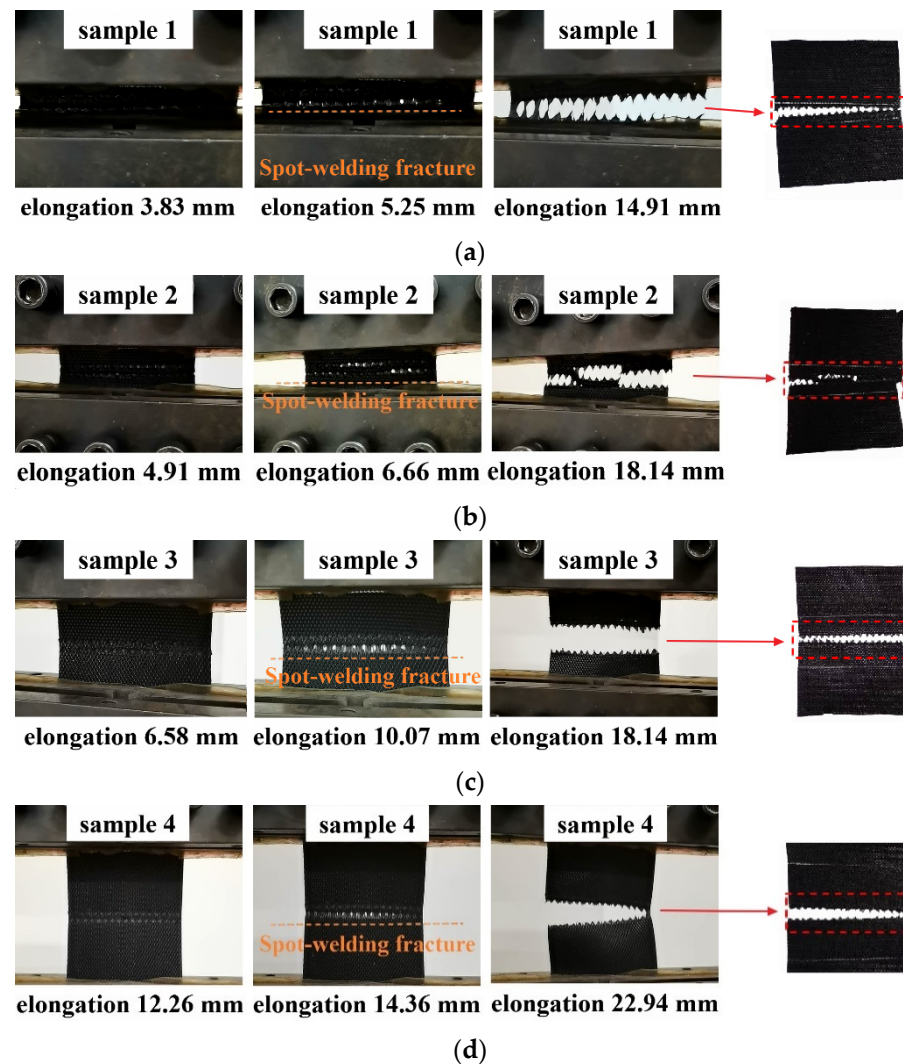


Figure 10. Failure modes of the junction subjected to uniaxial tension under various clamping distances: (a) 10.5 mm, (b) 25 mm, (c) 50 mm, (d) 100 mm.

3.2. Tensile Shear Test

The test results of different clamping distances under a shear force are summarized in Table 4. It can be seen that the shear strengths of the 25 mm, 50 mm, and 100 mm clamping distances are reduced by 3.44%, 9.25%, and 14.08% compared with the clamping distance of 10.5 mm. In terms of peak and overall elongation, the peak and overall elongation of the 25 mm clamping distance increased by 64.20% and 83.03% when compared with the 10.5 mm clamping distance. In comparison to the 25 mm clamping distance, the peak and overall elongation of the 50 mm clamping distance increased by 55.58% and 42.13%. Comparing the 50 mm clamping distance, the peak and overall elongation of the 100 mm clamping distance increased by 33.27% and 110.86%. In short, the junction shear strength decreases and the peak and overall elongation increase dramatically with the distance between clamps. It is worth noting that while the overall elongation growth was chaotic, the elongation growth with the peak decreases gradually.

Table 4. Tensile shear test results of the junctions.

Clamping Distance (mm)	Shear Strength (N·cm ⁻¹)	Peak Elongation (mm)	Overall Elongation (mm)
10.5	203.496	4.832	53.914
25	196.486	7.934	99.756
50	184.679	12.344	141.788
100	174.838	16.452	298.98

The plots of the shear stress–elongation of the junctions under different clamping distances are shown in Figure 11. It can be found that the peak and overall elongation both increase significantly with the distance between clamps. The majority of the tests showed similar results, and the peak strength varied only a little between samples with the same clamping distance. Firstly, the shear stress increased linearly before reaching its maximum value; then, it reached its maximum yield strength, and the strain-softening phenomenon appeared. The stress was reduced and then entered the major deformation stage, where the stress essentially stayed the same. Lastly, it entered the strain hardening stage, where the stress was raised and the sample was destroyed. The shear stress–strain behaviors became more similar to the standard tensile curve of the HDPE material strip as the distance between the clamps increased. However, there were differences in the failure area post-peak. Long deformation from the commencement of failure to complete failure is required for the test curve with a distance between clamps of 10.5 mm. The failure arises very suddenly when the distance between clamps is increased to 100 mm, but the two failure modes of the test curves of 25 mm and 50 mm both exist, which explains the problem of disordered overall elongation growth.

The failure modes of the samples under a shear force are shown in Figure 12. The results in Figure 12 indicate that the test procedure was characterized by apparent elongation deformation and a thin neck phenomenon of the strip. The two strips had no separation at the welding area, and the failures occurred at the connection between the welding junction and the strip. The welded junction is unlikely to fail when subjected to a shear force, and the actual shear strength of the junction should be higher than the shear yield stress obtained in the tests. It can also be found that the failure modes of the samples with a distance of 10.5 mm between the clamps were the ductile failure at the connection between the welded junction and the strip, and the increase in elongation caused the strip to separate from the junction (Figure 12a). Brittle failure appeared at the connection when the distance between the clamps was increased to 25 mm or 50 mm. The sample displayed a sudden general fracture failure after the elongation reached a specific degree (Figure 12b,c). When the clamping distance was increased to 100 mm, the sample failed as a result of a sudden brittle failure of the entire connection (Figure 12d). The reason for analyzing these fracture modes can be attributed to the characteristics of the welded junction. Two strips of ultrasonic spot welding form the welded junction, and the perforated area creates a weak area and is prone to stress concentration. The shear force of the junction becomes more like the tensile force on the strip as the clamping distance increases. The strip is stretched and hardened, and there are disparities in the changes at the junction, resulting in the sudden brittle failure of the connection between the junction and strip due to stress concentration.

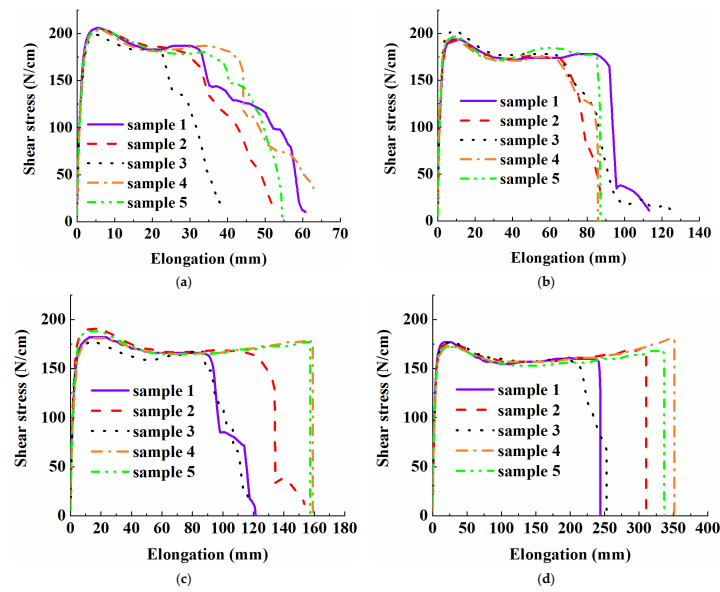


Figure 11. Shear stress–elongation relationship of the junction subjected to shear force under various clamping distances: (a) 10.5 mm, (b) 25 mm, (c) 50 mm, (d) 100 mm.

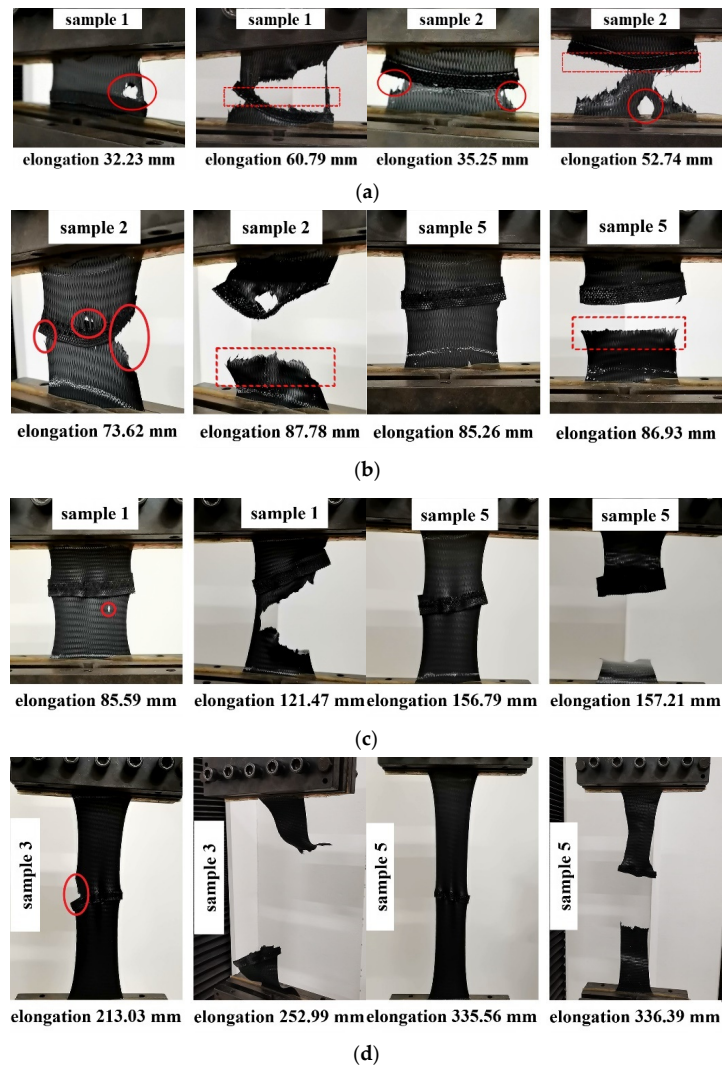


Figure 12. Failure modes of the junction subjected to shear force under various clamping distances: (a) 10.5 mm, (b) 25 mm, (c) 50 mm, (d) 100 mm.

In addition, the failure modes of the samples revealed the existence of strip damage (Figure 12a (sample 2) and Figure 12c (sample 1)). The different failure patterns can be attributed to the indented surface. According to Meuller, the surface structure of the HDPE composite influences its post-yielding behavior; more rapid failure can occur at the locations of stress concentration due to surface structural features, such as notches [24]. The deeper indentations served as the equivalent of notches for geocells. It is worth noting that these findings are consistent with the shear stress–elongation curve.

3.3. Peeling Test

Table 5 summarizes the peel strength testing results under a peeling force at different clamping distances. The peak elongation of the 50 mm clamping distance increased by 1.92%, and the overall elongation of the 50 mm clamping distance decreased by 2.45%, compared with the 25 mm clamping distance. Compared with the 50 mm clamping distance, the peak and overall elongation of the 100 mm clamping distance increased by 8.20% and 12.57%. As can be seen from the comparison, the overall elongation of the test samples fluctuates in a small range without evident change, and the peak elongation increases slightly with the change in clamping distance. The average peeling strengths of the 50 mm and 100 mm clamping distances were consistent, and the peeling strength of 25 mm is 3.15% lower. Therefore, the results of the junction peel strength test stay essentially with the increase in the distance between clamps.

Table 5. Peeling test results of the junctions.

Clamping Distance (mm)	Peeling Strength (N·cm ⁻¹)	Peak Elongation (mm)	Overall Elongation (mm)
25	106.27	14.592	27.33
50	109.62	14.872	26.66
100	109.62	16.092	30.012

Figure 13 exhibits the plots of the peel stress–elongation of the junctions under different clamping distances. All of the curves followed the same pattern. The peeling strength in the linear area pre-peak developed slowly and required more deformation, whereas the strength in the area post-peak rapidly diminished. Under the action of a peeling force, Figure 14 shows the failure process of samples with varying clamping distances. It can be seen that all the test samples failed in the same way, with the failures occurring at the connection between the junction and the strip, indicating that direct failure of the junction under the action of a peeling force is implausible. The welded junction is prone to material deterioration during the welding process, and stress concentration occurs at the perforated area, resulting in this failure mechanism.

Furthermore, some test results with considerable deviations were found during the experiment. The peel strength of these samples had decreased by 20% to 30%. They showed different fracture modes, and the welded-together strips were entirely separated at the junction. Figure 15 shows that the sample's welded junction had entirely separated due to the peeling force. Because this failure mode is uncommon, we consider it to be caused by the unqualified welding of the welded junctions during the production process.

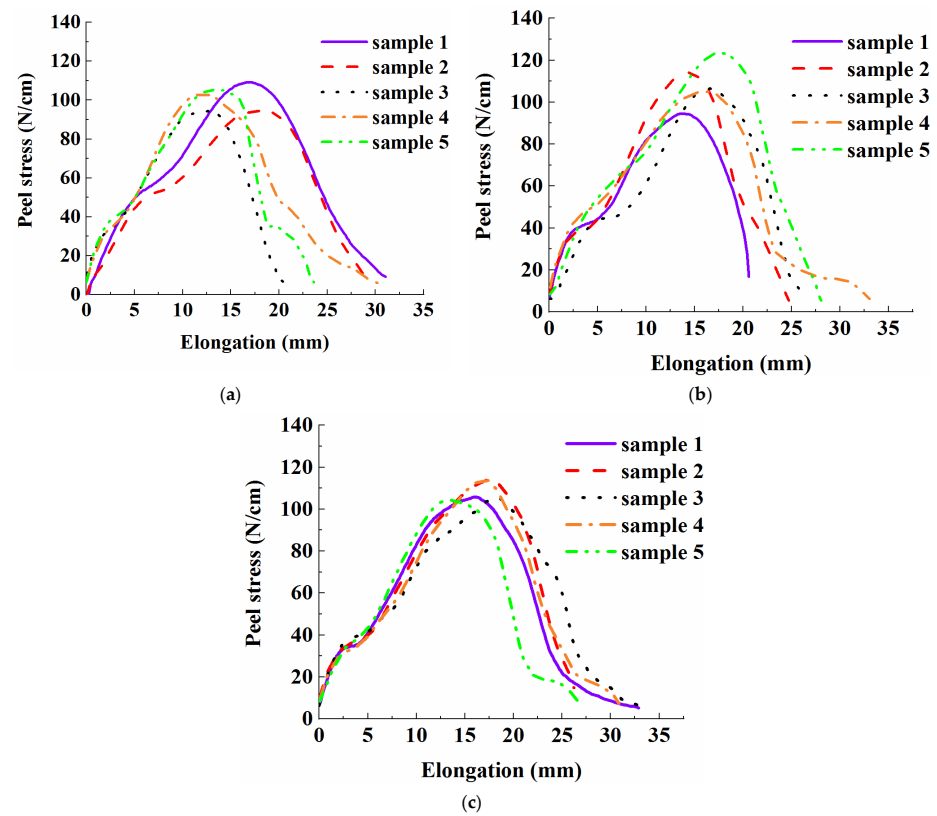


Figure 13. Peel stress–elongation relationship of the junction subjected to a peeling force under various clamping distances: (a) 25 mm, (b) 50 mm, (c) 100 mm.

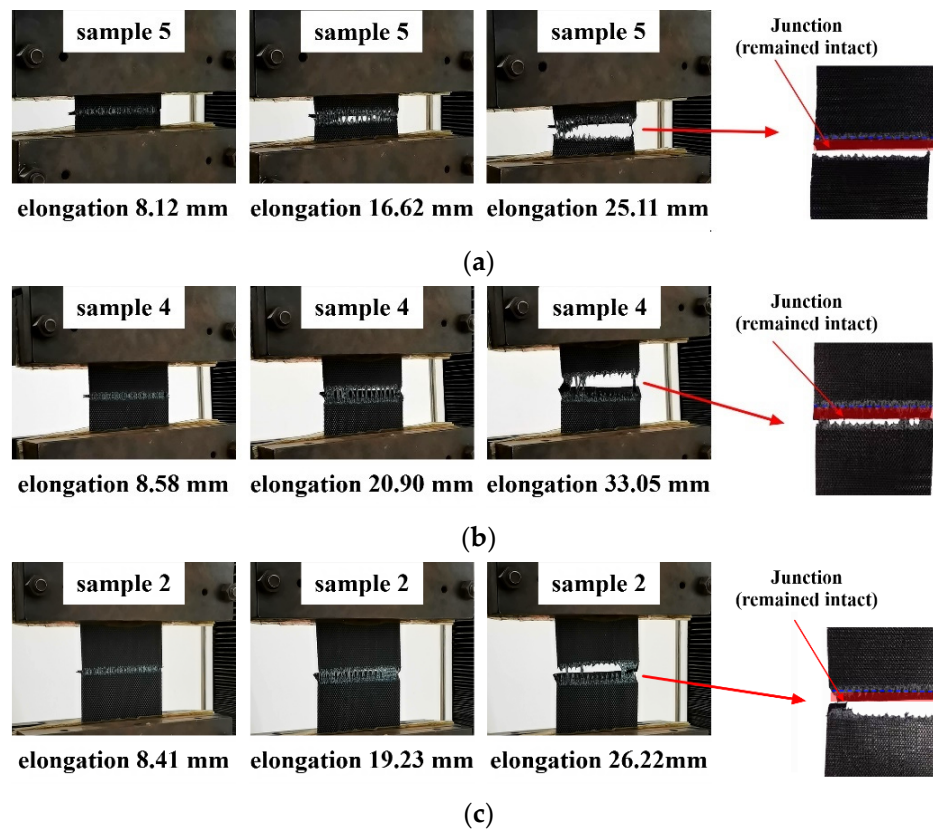


Figure 14. Failure modes of the junction subjected to a peeling force under various clamping distances: (a) 25 mm, (b) 50 mm, (c) 100 mm.

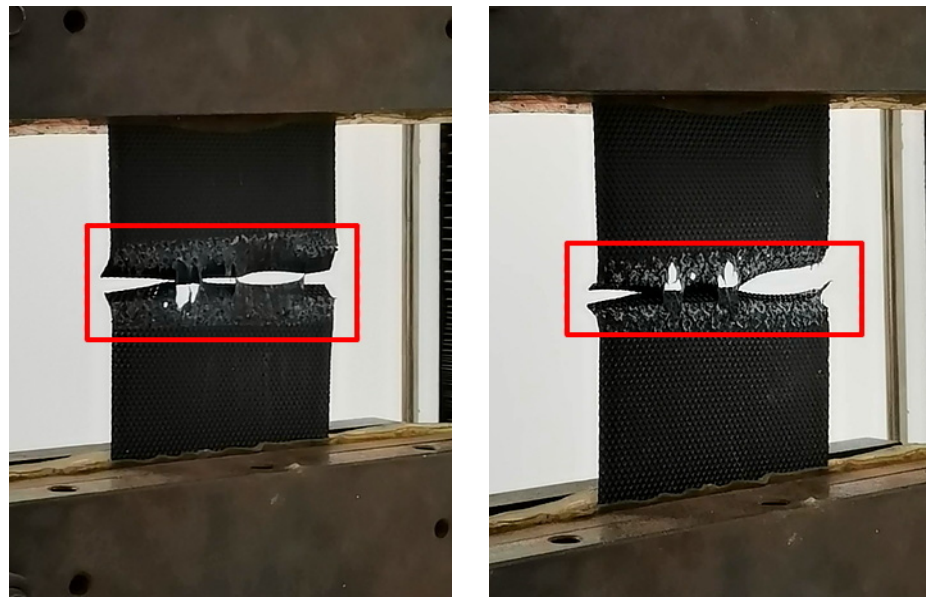


Figure 15. Weld fracture of the junction subjected to a peeling force.

3.4. Splitting Test

Table 6 shows the test results for the split strength of junctions at different clamping distances. The splitting strength of the 50 mm and 100 mm clamping distances increased by 0.10% and 1.3% compared to the 25 mm clamping distance. In terms of peak elongation, the peak elongation of the 50 mm clamping distance increased by 3% over the peak elongation of the 25 mm clamping distance. The peak elongation of the 100 mm clamping distance increased by 8.21% over the peak elongation of the 50 mm clamping distance. In terms of overall elongation, the overall elongation of the 50 mm is 7% less than the overall elongation of the 25 mm. The overall elongation of the 100 mm is 0.62% less than the overall elongation of the 50 mm. The splitting strength and elongation both increase or decrease slightly with a change in the clamping distance. Hence, increasing the distance between clamps has little bearing on the split strength test.

Table 6. Splitting test results of the junctions.

Clamping Distance (mm)	Splitting Strength ($\text{N}\cdot\text{cm}^{-1}$)	Peak Elongation (mm)	Overall Elongation (mm)
25	204.12	14.094	21.318
50	204.33	14.514	19.776
100	206.85	15.706	19.654

Figure 16 exhibits the graphs of the split stress–elongation of the junctions under different clamping distances. All of the results show a similar nature. The splitting strength in the linear area pre-peak increases slowly, and the strength in the area post-peak decreases more rapidly. This is consistent with the peeling strength test, indicating that the loading process is mostly similar between the two tests. The failure processes of the sample photographed are shown in Figure 17. The two welded strips separated, with progressive ductile failure and sudden brittle failure, which matched the test curve well.

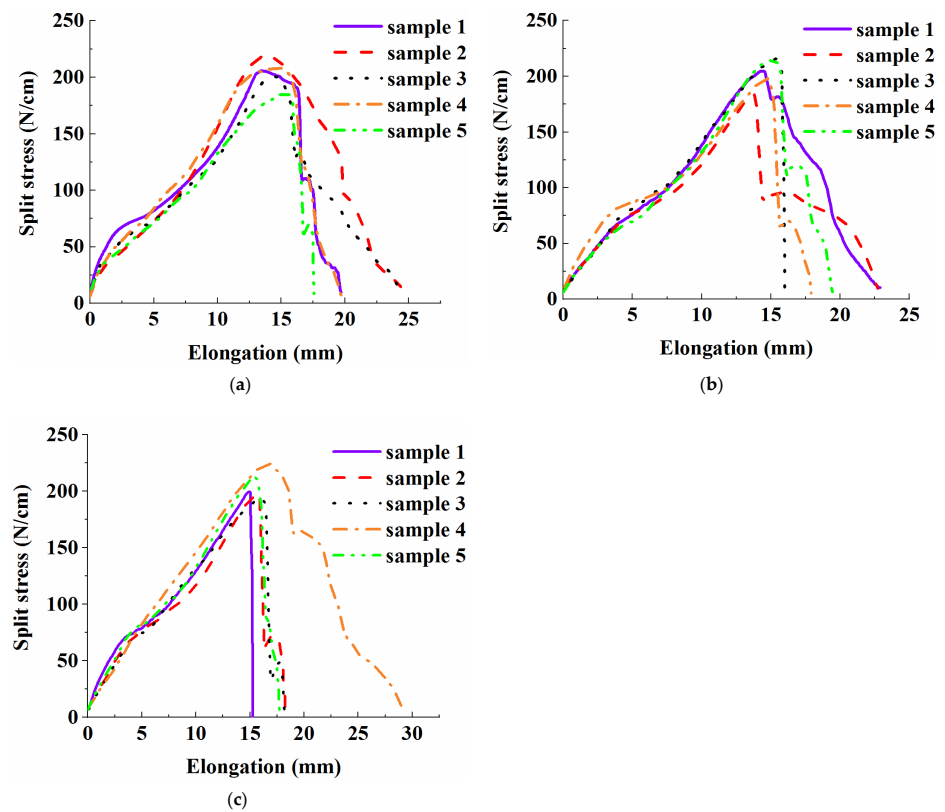


Figure 16. Split stress–elongation relationship of the junction subjected to a splitting force under various clamping distances: (a) 25 mm, (b) 50 mm, (c) 100 mm.

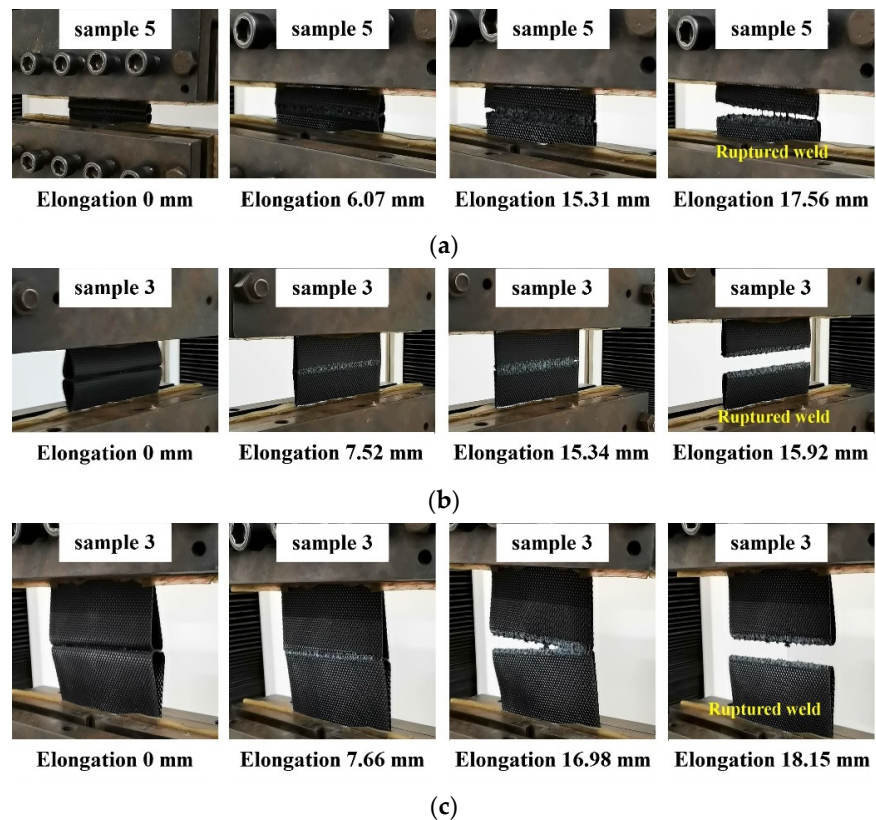


Figure 17. Failure modes of the junction subjected to a splitting force under various clamping distances: (a) 25 mm, (b) 50 mm, (c) 100 mm.

However, the experiment results showed various failure modes (Figure 18b). The sample failed at the junction between the two sides of the junction and the strip, which was identical to how the peeling strength test fails. This was due in large part to the sample's stress changing during the tensile process. It can be found from the test that the junction tilted under a splitting force (the red arrow in Figure 18a; the dashed line is the junction's initial direction), changing the force of the junction from a simple splitting force to a combination force of shear and splitting.

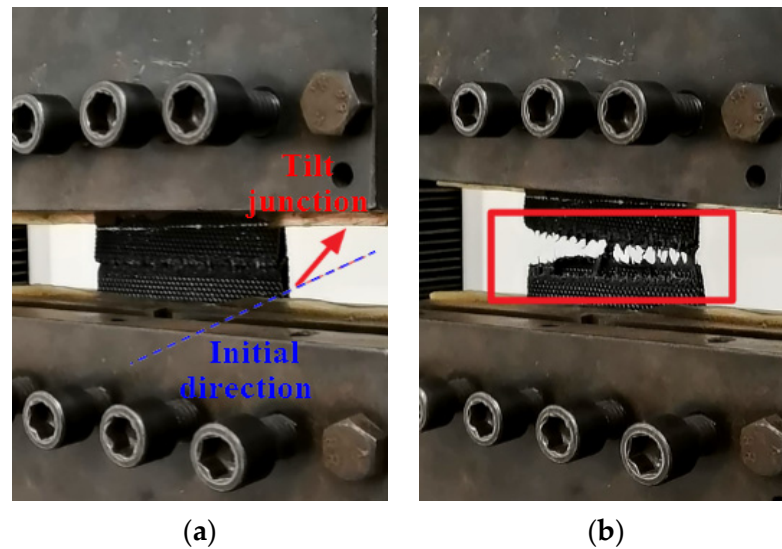


Figure 18. Different failure modes of the junction: (a) Directional change of the junction, (b) failure at the connection of the junction and the strip.

3.5. Comparative Analysis

For the junction tensile tests under the aforementioned four different stress states, Figures 19 and 20 show the geocell junction test results under different clamping distances in terms of strength and peak elongation. The possible failure modes of geocells in practical applications are analyzed, and the differences between different clamping distances are compared more clearly in order to provide more data support for test and practical engineering applications.

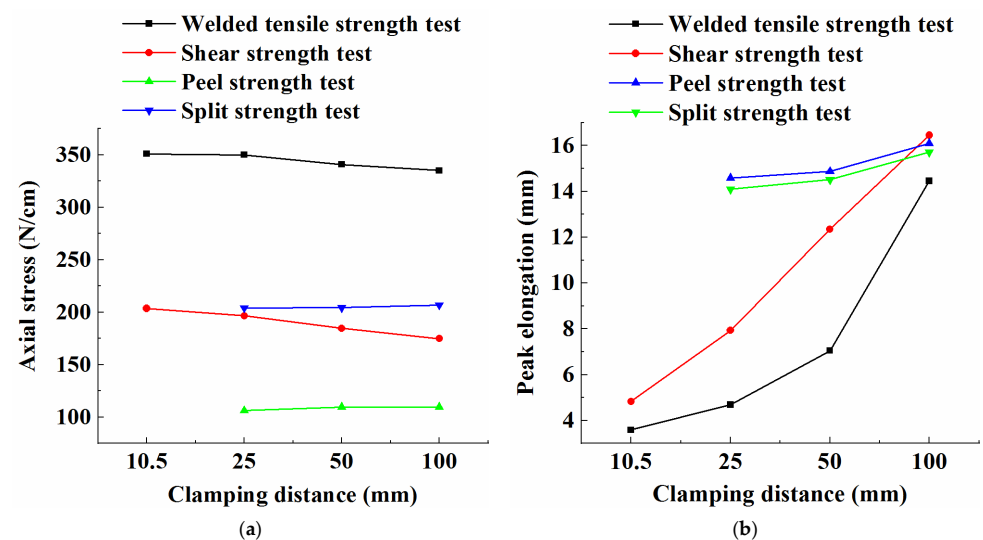


Figure 19. Junction test results under various clamping distances: (a) axial stress versus clamping distance; (b) pre-peak elongation versus clamping distance.

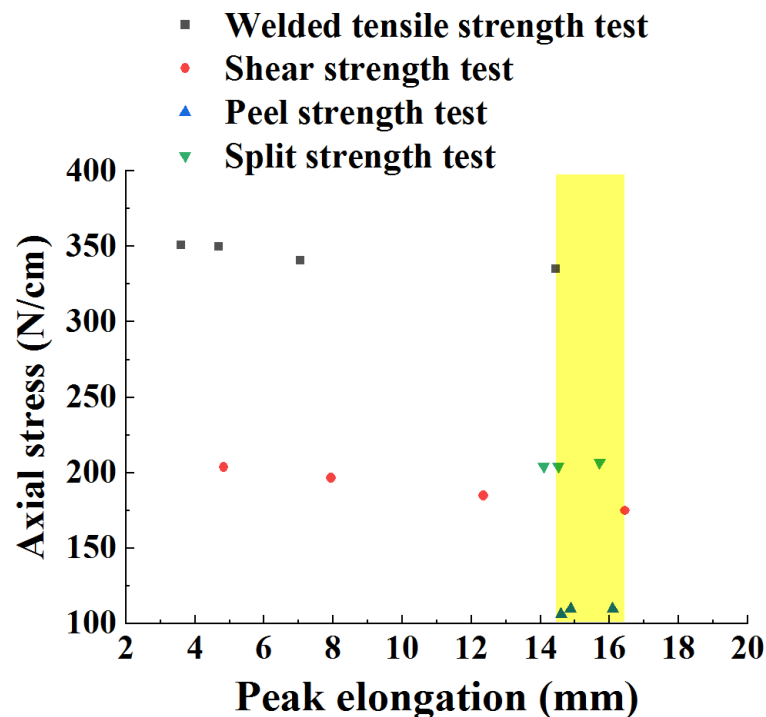


Figure 20. Junction test results under various clamping distances: axial stress versus peak elongation.

The tensile strength and shear strength of the junctions decrease slightly as the clamping distance increases, whereas the peeling strength and splitting strength stay almost unchanged, as seen in Figures 19a and 20. Overall, the yield strength of HDPE welded junctions under different stress states from high to low is: weld tensile strength, splitting strength, shear strength, and peeling strength. The failure modes of HDPE welded junctions in practical applications are mainly controlled by peel strength, which is consistent with the research [11,20,21]. Therefore, more attention should be paid to the control of the peeling force when the geocell of HDPE welded connections is employed in practical engineering.

The elongation required for four types of tests to attain peak strength increases with the clamping distance, as shown in Figure 19b, and the weld tensile and shear strength tests are more obviously affected by the strip. Comparing the four types of testing, the elongation required for the peel strength test to reach the peak is the largest at the 25 mm and 50 mm clamping distances; the peak elongation of the shear strength test is the largest at the 100 mm clamping distance. In addition, under the 100 mm clamping distance, there is minimal difference in the peak elongation of the tests (highlighted area in Figure 20). It is further confirmed that the peeling force is easily capable of causing geocell destruction.

There are anchor nails at the junctions of the geocells laid vertically along the slope, more filling pressure is dispersed to the depth of the slope through the anchor nails, and the junctions are subjected to the splitting force and weaken the peeling force. The junctions of the geocells laid along the horizontal direction of the subgrade are mainly subject to a peeling force, and rivets aggravate the peeling force. Therefore, the comprehensive analysis shows that the construction method of vertically laying down the slope is more reliable in the construction of geocell slope protection, which helps to improve the service life of geocells in slope protection.

4. Conclusions

A series of uniaxial tensile tests on the welded junctions of HDPE geocells was performed in this work, and the probable tensile force, shear force, peeling force, and splitting force of geocell junctions in practical applications were simulated. Firstly, the clamping distance of the current junction tensile test standard was explored, and the impact of

various clamping distances on the test was evaluated so as to provide a data basis and suggestions for establishing a new test standard. Then, their tensile strength, pre-peak, and post-peak behaviors were compared, and the failure modes under different loading types were observed. Finally, the influence of geocells lying on a slope in engineering was discussed.

This work draws the following conclusions:

- (1) The tensile strength of the weld tensile strength test decreases with the increase in the distance between clamps. The tensile strengths of the 100 mm clamping distance were decreased by 4.51% compared with the weld tensile strength test of the 10.5 mm clamping distance.
- (2) The shear strength of the tensile shear test decreases with the increase in the distance between clamps. The shear strengths of the 100 mm clamping distance were decreased by 14.08% compared with those of the 10.5 mm clamping distance. The pre-peak elastic and post-peak plastic area elongation both increased significantly.
- (3) The peel strength and split strength remain essentially unchanged with the increase in the distance between clamps. The elongation of the plastic area post-peak in the peeling test was 2.3 times that of the splitting test.
- (4) The peeling strength was the key determinant of whether HDPE welded junctions were damaged in practical applications. The elongation of the elastic area pre-peak in all the tests was similar at a 100 mm clamping distance.
- (5) Considering both strength and deformation, the construction method of geocells spreading vertically along the surface on a subgrade slope is thought to be more reliable, improving the service life of geocells in slope protection.

Author Contributions: Writing—review and editing, G.Y.; writing—original draft preparation, P.S.; validation, P.X., Z.W. and H.W.; methodology, Z.Z. All authors have read and agreed to the published version of the manuscript.

Funding: This research was supported by the National Natural Science Foundation of China (NSFC) (grants Nos. 52079078, 52108331 and 51709175), the Key R&D Projects in Hebei Province (grant No. 20375504D), the Hebei Provincial Department of Transportation Science and Technology Project (grant No. RW-202014), and the Scientific and Technological Research Projects of Colleges and Universities in Hebei Province (grant No. BJ2020045).

Institutional Review Board Statement: Not applicable.

Informed Consent Statement: Not applicable.

Data Availability Statement: The data used to support the findings of this study are available from the corresponding author upon request.

Conflicts of Interest: The authors declare no conflict of interest.

References

1. Wesołowski, M.; Włodarski, P.; Iwanowski, P.; Kowalewska, A. Analysis and assessment of the usefulness of recycled plastic materials for the production of airfield geocell. *Materials* **2021**, *14*, 3557. [[CrossRef](#)] [[PubMed](#)]
2. Wang, X.; Zhou, X.; Zhang, X. Laboratory Characterization of Geosynthetics-Reinforced Asphalt Mixture. *Materials* **2021**, *14*, 6424. [[CrossRef](#)]
3. Ahn, J.; Nguyen, T.H.; Yoo, I.K.; Oh, J. Investigation of Mechanical and Hydrologic Characteristics of Porous Asphalt Pavement with a Geocell Composite. *Materials* **2021**, *14*, 3165. [[CrossRef](#)] [[PubMed](#)]
4. Liu, Y.; Deng, A.; Jaksa, M. Three-dimensional modeling of geocell-reinforced straight and curved ballast embankments. *Comput. Geotech.* **2018**, *102*, 53–65. [[CrossRef](#)]
5. Gedela, R.; Kalla, S.; Sudarsanan, N.; Karpurapu, R. Assessment of load distribution mechanism in geocell reinforced foundation beds using Digital Imaging Correlation Techniques. *Transp. Geotech.* **2021**, *31*, 100664. [[CrossRef](#)]
6. Kargar, M.; Mir Mohammad Hosseini, S.M. Influence of reinforcement stiffness and strength on load-settlement response of geocell-reinforced sand bases. *Eur. J. Environ. Civ. Eng.* **2018**, *22*, 596–613. [[CrossRef](#)]
7. Liu, Z.; Liu, P.; Zhou, C.; Li, Y.; Zhang, L. Modeling Riverbank Slope Reinforcement Using Anti-Slide Piles with Geocells. *J. Mar. Sci. Eng.* **2021**, *9*, 394. [[CrossRef](#)]

8. Song, G.; He, S.; Song, X.; Duan, Z.; Zhang, Y.; Kong, D.; Huang, M. The use of geocell as soil stabilization and soil erosion countermeasures. *Geomat. Nat. Hazards Risk* **2021**, *12*, 2155–2169. [[CrossRef](#)]
9. Ari, A.; Misir, G. Three-dimensional numerical analysis of geocell reinforced shell foundations. *Geotext. Geomembr.* **2021**, *49*, 963–975. [[CrossRef](#)]
10. Hegde, A.; Sitharam, T.G. Joint strength and wall deformation characteristics of a single-cell geocell subjected to uniaxial compression. *Int. J. Geomech.* **2015**, *15*, 04014080. [[CrossRef](#)]
11. Isik, A.; Gurbuz, A. Pullout behavior of geocell reinforcement in cohesionless soils. *Geotext. Geomembr.* **2020**, *48*, 71–81. [[CrossRef](#)]
12. Khorsandiardebili, N.; Ghazavi, M. Static stability analysis of geocell-reinforced slopes. *Geotext. Geomembr.* **2021**, *49*, 852–863. [[CrossRef](#)]
13. Inti, S.; Tandon, V. Design of geocell reinforced roads through fragility modeling. *Geotext. Geomembr.* **2021**, *49*, 1085–1094. [[CrossRef](#)]
14. Zhao, Y.; Lu, Z.; Yao, H.; Zhang, J.; Yuan, X.; Cui, Y.; Nie, Y. Development and mechanical properties of HDPE/PA6 blends: Polymer-blend geocells. *Geotext. Geomembr.* **2021**, *49*, 1600–1612. [[CrossRef](#)]
15. Song, F.; Liu, H.; Hu, H.; Xie, Y. Centrifuge tests of geocell-reinforced retaining walls at limit equilibrium. *J. Geotech. Geoenviron. Eng.* **2018**, *144*, 04018005. [[CrossRef](#)]
16. Leshchinsky, B.; Ling, H. Effects of geocell confinement on strength and deformation behavior of gravel. *J. Geotech. Geoenviron. Eng.* **2013**, *139*, 340–352. [[CrossRef](#)]
17. Yang, X.; Han, J.; Pokharel, S.K.; Manandhar, C.; Parsons, R.L.; Leshchinsky, D.; Halahmi, I. Accelerated pavement testing of unpaved roads with geocell-reinforced sand bases. *Geotext. Geomembr.* **2012**, *32*, 95–103. [[CrossRef](#)]
18. Pokharel, S.K.; Han, J.; Leshchinsky, D.; Parsons, R.L.; Halahmi, I. Investigation of factors influencing behavior of single geocell-reinforced bases under static loading. *Geotext. Geomembr.* **2010**, *28*, 570–578. [[CrossRef](#)]
19. Vibhoosha, M.P.; Bhasi, A.; Nayak, S. A Review on the Design, Applications and Numerical Modeling of Geocell Reinforced Soil. *Geotech. Geol. Eng.* **2021**, *39*, 4035–4057. [[CrossRef](#)]
20. Zuo, Z.; Yang, G.Q.; Liu, Y.; Du, T.L.; Wang, Z.J.; Yu, F. Experimental investigations on failure mechanism of different junction connections of geocells. *Chin. J. Geotech. Eng.* **2021**, *43*, 1682–1690.
21. Liu, Y.; Deng, A.; Jaksa, M. Failure mechanisms of geocell walls and junctions. *Geotext. Geomembr.* **2019**, *47*, 104–120. [[CrossRef](#)]
22. Wu, K.J.; Austin, D.N. Three-dimensional polyethylene geocells for erosion control and channel linings. In *Geosynthetics in Filtration, Drainage and Erosion Control*; Elsevier: Amsterdam, The Netherlands, 1992; pp. 275–284.
23. Tariq, F.; Naz, N.; Khan, M.A.; Baloch, R.A. Failure analysis of high density polyethylene butt weld joint. *J. Fail. Anal. Prev.* **2012**, *12*, 168–180. [[CrossRef](#)]
24. Müller, W.W. *HDPE Geomembranes in Geotechnics*; Springer: Berlin, Germany, 2007; pp. 148–231.